arXiv:2105.00794v1 [eess.IV] 3 May 2021

ROBUST 3D CELL SEGMENTATION: EXTENDING THE VIEW OF CELLPOSE

Dennis Eschweiler[1], *Johannes Stegmaier*[1]

[1] Institute of Imaging and Computer Vision, RWTH Aachen University, Aachen, Germany

ABSTRACT

Increasing data set sizes of digital microscopy imaging experiments demand for an automation of segmentation processes to be able to extract meaningful biomedical information. Due to the shortage of annotated 3D image data that can be used for machine learning-based approaches, 3D segmentation approaches are required to be robust and to generalize well to unseen data. Reformulating the problem of instance segmentation as a collection of diffusion gradient maps, proved to be such a generalist approach for cell segmentation tasks [1]. In this paper, we extend the Cellpose approach to improve segmentation accuracy on 3D image data and we further show how the formulation of the gradient maps can be simplified while still being robust and reaching similar segmentation accuracy. We quantitatively compared different experimental setups and validated on two different data sets of 3D confocal microscopy images of *A. thaliana*.

***Index Terms*—** Cellpose, 3D Segmentation, Generalist.

1. INTRODUCTION

Current developments in digital microscopy allow to generate image data with progressively increasing resolution and often accordingly increasing data size. Especially in 3D microscopy, data sizes often lie within the terabyte range, which requires a high degree of automation of analytical processes including segmentation tasks [2]. Machine learning-based segmentation approaches require annotated training data sets for reliable and robust outcomes, which, however, are rarely available. This issue is even more severe for 3D microscopy image data, since manual annotation of 3D cellular structures is very time-consuming and often infeasible, which causes the acquisition of annotated 3D data sets to be highly expensive.

On the one hand, 2D approaches have been applied in a slice-wise manner to overcome this issue [1], diminishing the need for expensive 3D annotations, but resulting in additional sources of errors and inaccuracies. Segmentation errors are more likely to occur at slice transitions, leading to noisy segmentations, and omitting information from the third spatial dimension, *i.e.*, a decreased field of view, leads to a potential loss of segmentation accuracy. On the other hand, if there are fully annotated 3D data sets available, robust and generalist approaches are desired to make full use of those data sets.

In the recent past, Stringer *et al.* proposed the Cellpose algorithm [1] and demonstrated that this approach serves as a reliable and generalist approach for cellular segmentation on a large variety of data sets. However, this method was designed for a 2D application and although a concept to obtain a 3D segmentation from a successive application of the 2D method in different spatial dimensions was proposed, the approach is still prone to the aforementioned sources of errors, missing on the full potential for 3D image data. In this paper we propose (1) an extension of the Cellpose approach to fully make use of the 3D information for improved segmentation smoothness and increased robustness. Furthermore, we demonstrate (2) how the training objective can be simplified without loosing accuracy for segmentation of fluorescently labeled cell membranes. (3) Generalizability is assessed on 3D microscopy image data of four different data sets.

2. METHOD

The proposed method extends the Cellpose algorithm proposed by Stringer *et al.* [1], which formulates the instance segmentation problem as a prediction of directional diffusion distributions within a cell. These distributions are modelled as heat diffusion, originating at the center of a cell and extending to the cell boundary, leading to spatial gradients that can be derived from this process (Fig. 1, upper row). Gradients are divided into separate maps for each spatial direction, which can then be predicted by a neural network alongside a foreground prediction map that is used for excluding background gradients from further calculation. After prediction of the foreground and gradient maps using a U-Net architecture [3], each cell instance is reconstructed by tracing the multi-dimensional gradient maps to the respective simulated heat origin. All voxels that end up in the same sink are ultimately assigned to the same cell instance.

For processing images directly in 3D, some processes need to be simplified in order to overcome memory shortages and to prevent long run-times. First, we propose to use a simplified objective for the generation of the gradient maps, since calculation of a heat diffusion in 3D is computationally expensive. Note that the simplification is a trade-off between

We thank the German Research Foundation DFG for funding (DE, Grant No STE2802/2-1). Correspondence: {dennis.eschweiler, johannes.stegmaier}@lfb.rwth-aachen.de

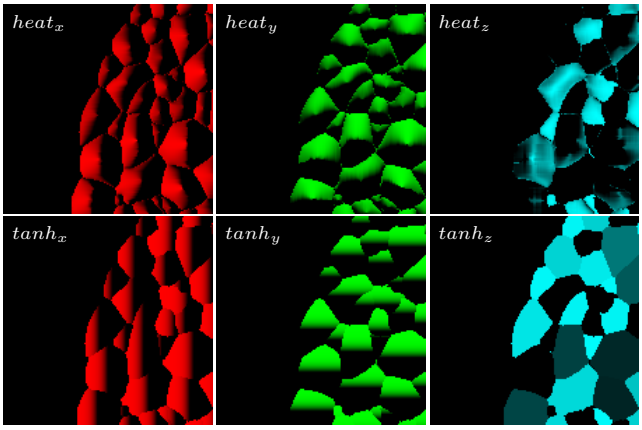

Fig. 1. Gradient map representation of cell instances in x (red), y (green) and z (blue) directions. The upper row shows heat diffusion simulations [1], while the lower row shows the simplified hyperbolic tangent distributions. Brightness indicates the gradient direction.

lower complexity and the ability to reliably segment overly non-convex cell shapes. For most of our applications related to segmentation of fluorescently labeled cell nuclei or membranes from images of early developmental processes, however, this simplification is justified by having almost only convex objects. Instead of computing a complex heat diffusion process, we rely on a hyperbolic tangent spanning between cell boundaries in each spatial direction (Fig. 1, lower row). Predictions are obtained by a 3D U-Net [4], including all of the three spatial gradient maps for the x, y and z direction, respectively, and the additional 3D foreground map highlighting cellular regions. Since the training objective is formulated by a hyperbolic tangent, the output activation of the U-Net is set to a hyperbolic tangent accordingly. Processing images directly in the 3D space has the advantage of performing predictions only once for the entire stack, as opposed to a slice-wise 2D application, which has to be repeated multiple times along each axis to obtain precise gradient maps for each spatial direction.

Reconstruction of cell instances is done in an iterative manner, by moving each voxel within the foreground region along the predicted gradient field by a step size δ_{recon}, given by the magnitude of the predicted gradient at each respective position. The number of iterations is defined by a fixed integer N_{recon}, which is adjusted by the presumed average cell radius r_{cell} and, thus, the maximum number of steps necessary to move a boundary voxel to the cell center. Ultimately, each voxel ends up in the vicinity of the corresponding cell center and can be assigned the respective cell id.

As a second simplification, we design the assignment of voxels to individual cell instances based on mathematical morphology, which enables a fast processing independent from the potentially large quantity of cells in 3D image data. Rather than applying clustering techniques on the single voxel level, this allows a constant time consumption of the assignment process and consequently yields a constant and faster run-time of the algorithm. A morphological closing operations using a spherical structuring element with a radius of half the estimated average cell radius r_{cell} are applied to determine unique cell clusters in form of connected components. After assignments, each voxel is backtracked to its original position and labeled with the id of the assigned connected component, resulting in the final instance segmentation.

3. EXPERIMENTS AND RESULTS

To evaluate our method, we conducted four different experiments on the basis of the publicly available data set from [5]. The data set includes 125 3D stacks of confocal microscopy image data showing fluoerescently labeled cell membranes in the plant model organism *A.thaliana*. We divided the data set into training and test sets, where plants 1,2,4 and 13 were used for training and plants 15 and 18 were used for testing. The test data set comprises about 37000 individual cells. The experiments are structured as follows:

Exp1 As a baseline we used the publicly available pretrained Cellpose *cyto*-model [1] and applied it to the test data set. Since the model was trained on a large and highly varying data set, we did not perform any further training.

Exp2 The second experiment was designed to be a second baseline, as we used the original Cellpose approach [1] and trained it from scratch for 1000 epochs with the abovementioned Meristem training data set. To reduce memory consumption and prevent high redundancies, we extracted every fourth slice of each 3D stack of the training data set to construct the new 2D training data. In combination with the first experiment, this shows how well the approach performs when applied to a similar data set as the one it was trained on.

Exp3 Our proposed 3D extension was first trained with the original representation of the gradient maps, formulated as a heat diffusion process [1]. The 3D U-Net was trained on patches of size $128 \times 128 \times 64$ voxel for 1000 epochs using the Meristem training data set. During every epoch, one randomly located patch was extracted from each image stack of the training data set. To obtain the final full-size image, a weighted tile merging strategy as proposed in [6] was used on the predicted foreground and gradient maps, before reconstructing individual instances.

Exp4 For the fourth experiment, we used the simplified representation of the gradient maps, formulated by hyperbolic tangent functions as described in Sec. 2. Otherwise, the

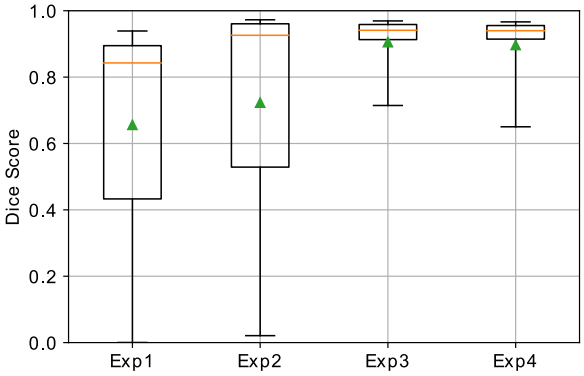

Fig. 2. Dice scores computed from segmentation results obtained for the public Meristem data set [5] by each experiment, including pretrained Cellpose provided by [1] (Exp1), a retrained version of the original Cellpose architecture (Exp2), our 3D extension with the original (Exp3) and the simplified (Exp4) gradient formulation.

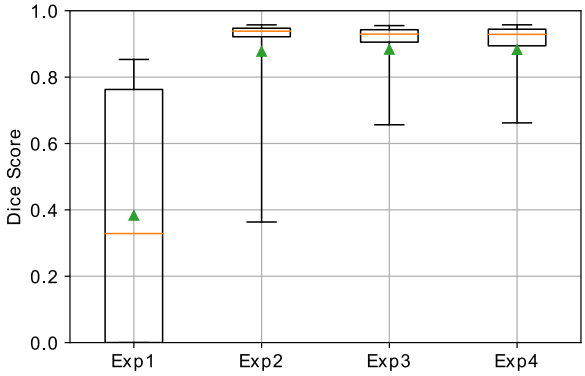

Fig. 3. Dice scores computed from segmentation results obtained for the manually annotated 3D image stack. The methods include the pretrained Cellpose provided by [1] (Exp1), a retrained version of the original Cellpose algorithm (Exp2), our approach with the original (Exp3) and the simplified (Exp4) gradient formulation.

training setup is identical to the setup of experiment Exp3.

To assess the segmentation accuracy, a Dice score was used as a metric, which we illustrate as boxplots in Fig. 2. Whiskers represent the 5th and 95th percentile, respectively, the box spans from the 1th to the 3rd quartile, the orange line shows the median value and the green triangle indicates the mean value. Final mean Dice values are 0.656 for Exp1, 0.723 for Exp2 and 0.905 and 0.897 for Exp3 and Exp4, respectively. Qualitative segmentation results are illustrated in Fig. 4, showing 2D slices of a raw image patch and the corresponding instance segmentation ground truth in comparison to segmentation results obtained with each of the experimental setups. Overall, the native pseudo-3D Cellpose approaches (Exp1 and Exp2) suffer from low-quality and missing instance segmentations in regions with low fluorescence intensity, leading to a large spread of obtained segmentation scores. The full 3D approaches (Exp3 and Exp4), however, are able to exploit the structural information from the third dimension to successfully outline cell instances despite the low intensity. Final results show that similar segmentation quality is obtained from both gradient field formulations with a small trade-off between segmentation accuracy and gradient complexity.

Furthermore, we wanted to show how well each of the approaches performs on data from an entirely different data set to assess the ability to generalize to different microscopy settings. Therefore, we used a manually annotated 3D confocal stack of *A. thaliana*, comprising a total of 972 fully annotated cells. Annotations were manually obtained using the SEGMENT3D online platform [7] and we again used a Dice score as a metric to assess the segmentation quality of each of the conducted experiments. Results are shown as boxplots in Fig. 3. The final mean Dice scores are 0.383 for Exp1, 0.877 for Exp 2 and similar scores of 0.883 for both, Exp3 and Exp4. Representative 2D slices showing the raw image with corresponding ground truth segmentation and the segmentation results of each experiment are illustrated in Fig. 5. Results obtained with Exp1 show again that the lack of structural 3D information leads to a loss of segmentation accuracy, especially in regions of ambiguous intensity patterns of cell membranes. Approaches directly trained on a similar data set (Exp2-Exp4) perform similarly well and demonstrate an increased segmentation accuracy in difficult regions. Nevertheless, Exp2 still exposes a loss of segmentation accuracy when not making use of the full 3D information.

4. CONCLUSION

In this work we demonstrated how the concept of the generalist instance segmentation approach Cellpose [1] exploiting instance gradient maps can be extended to increase segmentation accuracy for 3D image data. The inclusion of information from the third dimension, *i.e.*, by directly operating on 3D patches to predict instance gradient maps, helps to improve segmentation of cells in regions of poor image quality and low intensity signals. The simplification of the proposed instance gradient maps leads to a comparable accuracy of segmentation results, while offering a lower complexity in the gradient formulation. Results obtained with an approach trained on a completely different data set support the claim of this approach to be generalist and robust. We could additionally show the generalist property for the proposed 3D

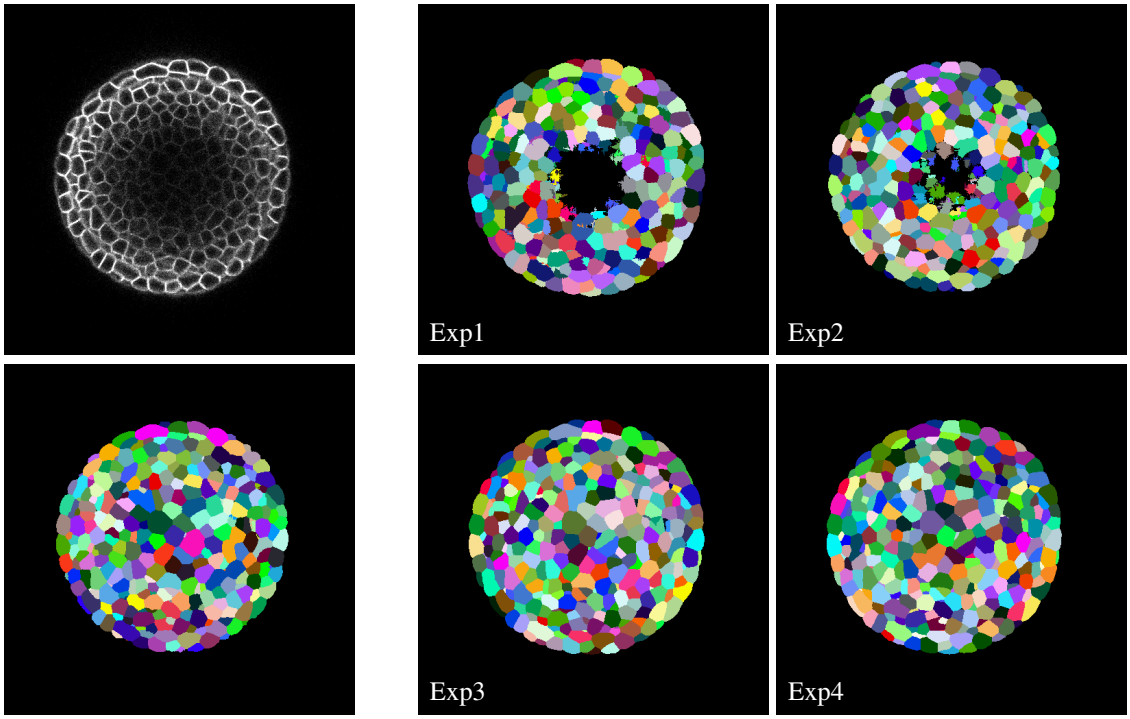

Fig. 4. 2D slices of raw images and ground truth segmentation of the public 3D data set [5], alongside segmentation results obtained with pretrained Cellpose provided by [1] (Exp1), Cellpose trained on the public data set [5] (Exp2), our approach with the original (Exp3) and the simplified (Exp4) gradient formulation.

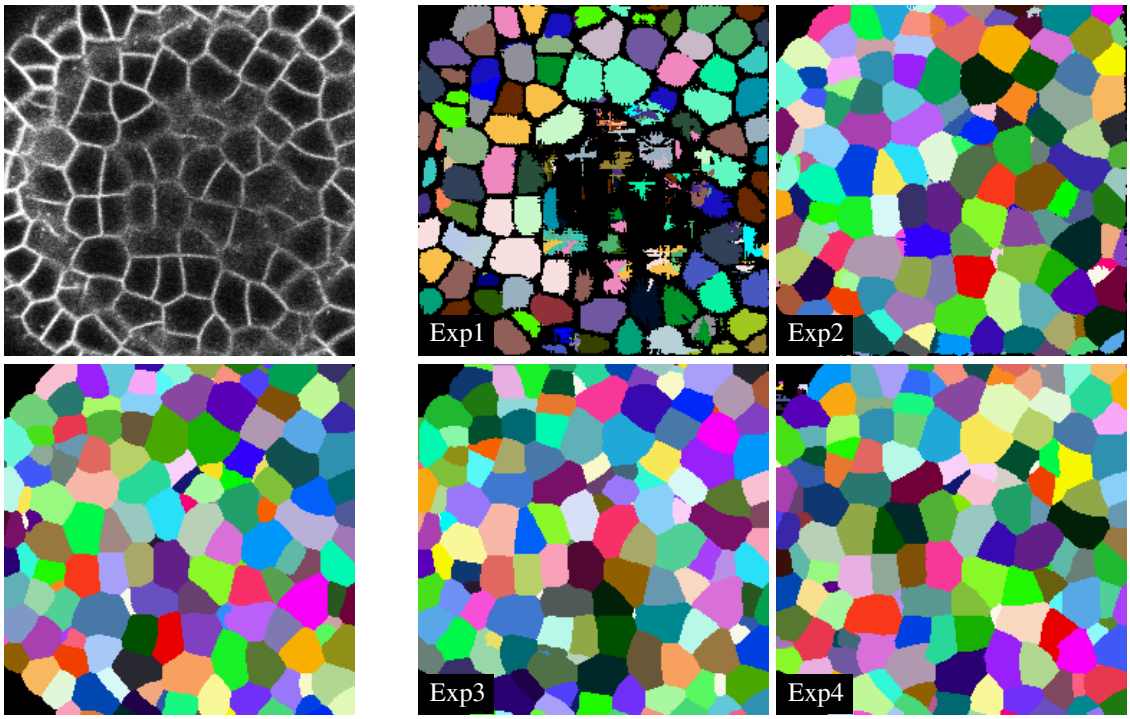

Fig. 5. 2D slices of raw images and ground truth segmentation of the manually annotated 3D image stack, alongside segmentation results obtained with pretrained Cellpose provided by [1] (Exp1), Cellpose trained on the public data set [5] (Exp2), our approach with the original (Exp3) and the simplified (Exp4) gradient formulation.

extension of Cellpose on a different data set. Future work will include an improvement of the iterative instance reconstruction, which is still the computational bottleneck of the segmentation pipeline.

5. REFERENCES

[1] C. Stringer, T. Wang, M. Michaelos, and M. Pachitariu, "Cellpose: a Generalist Algorithm for Cellular Segmentation", *Nature Methods*, vol. 18, no. 1, pp. 100–106, 2021.

[2] E. Meijering, "A Bird's-Eye View of Deep Learning in Bioimage Analysis", *Computational and Structural Biotechnology Journal*, vol. 18, pp. 2312, 2020.

[3] O. Ronneberger, P. Fischer, and T. Brox, "U-Net: Convolutional Networks for Biomedical Image Segmentation", in *International Conference on Medical Image Computing and Computer-Assisted Intervention*, 2015, pp. 234–241.

[4] Ö. Çiçek, A. Abdulkadir, S. S. Lienkamp, T. Brox, and O. Ronneberger, "3D U-Net: Learning Dense Volumetric Segmentation from Sparse Annotation", in *International Conference on Medical Image Computing and Computer-Assisted Intervention*, 2016, pp. 424–432.

[5] L. Willis, Y. Refahi, R. Wightman, et al., "Cell Size and Growth Regulation in the Arabidopsis Thaliana Apical Stem Cell Niche", *Proceedings of the National Academy of Sciences*, vol. 113, no. 51, pp. E8238–E8246, 2016.

[6] D. Eschweiler, M. Rethwisch, S. Koppers, and J. Stegmaier, "Spherical Harmonics for Shape-Constrained 3D Cell Segmentation", in *IEEE International Symposium on Biomedical Imaging*, 2021.

[7] T. V. Spina, J. Stegmaier, A. X. Falcão, E. Meyerowitz, and A. Cunha, "SEGMENT3D: A Web-based Application for Collaborative Segmentation of 3D Images used in the Shoot Apical Meristem", in *IEEE International Symposium on Biomedical Imaging*, 2018, pp. 391–395.